

Uneven surface moisture as a driver of dune formation on ephemeral lake beds under conditions similar to the present day: a model-based assessment from the Makgadikgadi basin, northern Botswana.

Abstract

An association between salt pans or dry lake beds and distinctive crescentic lake-floor sand mounds (1-10m high, 10s - 100s m wide) are commonplace in desert systems. In the Makgadikgadi basin of northern Botswana a debate about the formative processes of these landforms has persisted despite numerous morphometric, sedimentary and geochronological analyses, with mound landforms variously inferred to be aeolian dunes, subaqueous dunes, spring mounds, or shoreline remnants. We propose a new formative mechanism which draws on the interaction between uneven moisture distribution on the pan surface and mobile aeolian sediments. We use a numerical model (ViSTA), which couples vegetation and aeolian sand transport dynamics, together with Optically Stimulated Luminescence (OSL) dating of a mound in the Makgadikgadi basin to investigate the feasibility of this “sticky mound hypothesis”. We find that under a range of modelled environmental conditions, uneven moisture distribution on the pan surface can lead to the development and stabilisation of crescentic aeolian dunes, with these dunes growing upwind from the point of initial deposition, corresponding with the chronological data gained from OSL dating of a mound feature. On removal of this moisture, the modelled dunes erode and dissipate. These findings suggest that the formative mechanism of the mounds could be dependent on the interaction between differential drying of the pan surface and the competence of the aeolian sediment transport system across the pan floor.

Key words: lake bed dunes; paleoenvironment; landscape development; cellular automata; aeolian sand transport; drylands

1 Introduction

There are a variety of geomorphological relationships between aeolian dunes and lake basins particularly within dryland systems (Goudie and Thomas, 1986; Lancaster, 1978), but one of the most enigmatic of these associations surrounds the identification of crescentic or sinuous lake floor dunes/mounds within dry or ephemeral lake beds and salt pans. These have been identified in a number of basins globally (Burrough et al., 2012) including Lake MacKay and Lake Amadeus in Australia and Lake Chad, the Makgadikgadi Pans and Etosha Pans in Africa (Figure 1). In some cases, they have been dated to make inferences about past lake levels and palaeoclimate change (e.g. in Lake Chad, Grove and Warren, 1988; Armitage et al., 2016). However, globally, there has been little systematic analysis of these landforms but they offer potential significance as geoproxies for lacustrine hydrological changes through geomorphological and geochronological constraints on lake floor sediments (e.g. Bristow et al., 2009; Burrough and Thomas, 2013; Grove, 1969). Similar intra-basin crescentic landforms have also been identified on the surface of Mars (Franchi et al., 2014; Pondrelli et al., 2015, 2019; Pozzobon et al., 2019) and knowledge of their formative mechanisms may help landscape interpretation in this extra-planetary context (e.g. Bourke and Goudie, 2009; Franchi et al., 2020). One region, the Makgadikgadi basin of northern Botswana, has received notable long-term interest and investigation into the formation of these landforms (e.g. Cooke, 1980; Grey and Cooke, 1977; Grove, 1969). Here, scientific interest in the crescentic sand mounds has spanned half a century and the unresolved debate concerning their origins has become increasingly lively in recent years (e.g. Burrough et al., 2012; Burrough and Thomas, 2013; Franchi et al., 2020; McFarlane and Long, 2015). In this paper we take aspects of these previous empirical studies to inform a model-based approach that tests the feasibility and robustness of a new theory of formation; “the sticky mound hypothesis”.

1.1 *The Makgadikgadi Basin*

Formerly one of Africa's largest lakes, the Makgadikgadi basin in northern Botswana consists of ca. 16,000 km of interconnected salt pans. The margins of the lake basin are demarcated by the accumulation of wave transported sediments that formed beach ridges during lake high-stands in the late Quaternary (Burrough et al., 2009), with regions of these shorelines impacted by neo-tectonism (Eckardt et al., 2016). The basin is underlain by a doleritic dyke swarm (Elburg and Goldberg, 2000) trending ESE-WNW above which Kalahari Group bedrock deposits lie with a thickness of between 50 and 300 m (Thomas and Shaw, 1991). The interaction between the subsurface geology and surface moisture/flooding is poorly understood. Today, seasonal rainfall, surface and subsurface flow, can flood the salt pan to a maximum depth of ~1 m (Burrough et al., 2012). There is strong inter-annual variation in surface flooding but topography also plays a role with lower regions of the basin in the east (particularly within Sua Pan) being submerged more frequently over a 10 year period than topographically higher areas in the west of the basin (Ntwetwe Pan) (Bryant et al., 2007). Overall, however, the system maintains a negative water balance for most of the year due to excessive evaporative losses. Following seasonal rainfall or flood events, the water table remains shallow and, as the pan surface dries out, consolidated evaporitic surface crusts form across much of the basin floor. These evaporitic crusts are principally composed of halites derived from the evaporation of sodium chloride brines (Eckardt et al., 2008). Crusts can form smooth polygonal patterns limiting subsurface exposure but are dynamic over the course of a seasonal cycle and can become ridged and cracked, enabling exchange between surface and subsurface processes particularly in terms of sediment availability (Nield et al., 2015). Interactions between exposed sediment and aeolian processes result in the Makgadikgadi pan being a major dust hot spot, with the extent of dust loadings being influenced by a range of factors including wind speed and sediment supply to the pan (Bryant et al., 2007; Nield et al., 2015). Dust emission from the surface is in part triggered by the saltation impacts of larger, particles on

the surface (Neild et al., 2015), which in turn can drive the erosion, transportation and deposition of sediment across the pan surface. The pan surface can become 'reset' to a flatter, continuous crust through seasonal flooding and/or a return to a high-water table (Neild et al., 2015), although sediment mounds higher than the water depth can persist in spite of the seasonal flooding.

1.2 Mound distribution, formation and controversy

Locally referred to as 'islands', crescentic to near-circular, vegetated accumulations of unconsolidated sand stand several meters above the saline lake floor with a typical concentric zonation or tone-banding (Figure 1d). The mounds are found widely across the basin but dominate the drier, downwind western side of the Ntwetwe Pan. Elsewhere mounds tend to be more sporadic, located in less frequently inundated areas towards the eastern margins of the Ntwetwe panhandle and on Sua Pan. Some form distinct arcuate shaped mounds whilst others are more elongate in form. Previous investigations suggest they are primarily composed of poorly sorted, very fine to medium sand-sized particles (Burrough et al., 2012; Franchi et al., 2020, Burrough et al., in prep). Their vegetated surfaces, which can sustain a dense covering of halotrophic grasses (pre-dominantly *Odyssea paucinervis* and *Sporobolus ioclados*), make these features visibly distinct in remotely sensed imagery, in contrast to the generally de-vegetated and inhospitably saline conditions of the pan floor (Burrough et al., 2012). In some areas on the pan floor, it is also possible to identify mound 'footprints', crescentic shaped imprints on the pan floor marked by hardened silcretised sands and/or granule lag deposits but without any clear topographic expression (e.g. Figure 2). Possible mechanisms for the decay of mounds might include the loss of stabilizing vegetation due to submersion by saline floods or a prolonged period of aridity, loss of moisture below the mound, or increased erosivity due to changes in wind strength and frequency.

92 Occurring consistently transverse to the currently prevailing easterly wind, Grove (1969) referred to
93 these features as *barchan dunes*. He argued that the concentric zonation of their margins was due to
94 benching or terracing during periods of shallow lake-floor flooding. The attribution of an aeolian origin
95 was subsequently disputed by Cooke (1980) who alternatively hypothesised a subaqueous origin,
96 formed during lake high stands in the late Quaternary. More recently, Burrough et al. (2012) and
97 Burrough and Thomas (2013) undertook a detailed analysis using morphometric measurements,
98 sedimentary data, and Optically Stimulated Luminescence (OSL) dating and luminescence signal
99 analyses. They were unable to definitively attribute the mounds to a clear formative environment,
100 though their consistent late Holocene ages lent support to an aeolian origin and they tentatively
101 suggested the mounds were indeed barchans. In an alternative assessment, using Google Earth imagery,
102 McFarlane and Long (2015) inferred the features to be *spring mounds* formed by ongoing discharge of
103 potable groundwater and sediment, with their initiation related to a pre-Quaternary lake. Most recently
104 Franchi et al. (2020) used electric resistivity tomography (ERT) to assess water upwelling processes and
105 found the presence of a highly resistive body (the mound sediments) over a low resistivity body, possibly
106 linked to a capillary fringe or very shallow groundwater table within the lake bed sediments. Franchi et
107 al. (2020) also reached no firm conclusion but suggested the ‘layered mounds’ were remnants of the
108 lake’s former shoreline, the result of progressive erosion by surface runoff and wind deflation of relict,
109 bedded strandlines.

110 Each of these explanations for the origin of the crescentic mounds carries significant implications for
111 understanding landscape evolution in the basin. From the perspective of past climatic conditions, the
112 formation of aeolian barchan dunes on the Makgadikgadi lakebed (and other lakebeds globally) would
113 imply these landforms are indicative of dry times in the lake basin (e.g. Burrough and Thomas, 2013), as
114 compared to their interpretation as sub-aqueous dunes inferring the presence of a large palaeolake (e.g.
115 Cooke, 1980). The mounds’ association with well-preserved Middle Stone Age sites in the basin

(Burrough et al., 2018) adds further archaeological significance for understanding their formative mechanism. Conversely, a spring mound hypothesis (McFarlane and Long, 2015), has important consequences for managing present-day water resources and wildlife stocking capacity within the Makgadikgadi National Park, a particularly fragile ecosystem that overlaps with the densest occurrence of mounds in western Ntwetwe Pan.

Franchi et al. (2020) suggest they are comparable to landforms identified within the Firsoff impact crater on Mars (Franchi et al., 2014) (Figure 1f), with the inference that the potential role of liquid water in the formation and preservation of the Makgadikgadi mounds has implications for interpreting past and present conditions within Martian landscapes. So, whilst the Makgadikgadi mounds hold a relatively obscure position within a geomorphological context, resolving the mechanism of their formation has direct relevance for the interpretation of landscape scale hydroclimates past, present, and extraterrestrial.

1.3 The Sticky Mound Hypothesis

While we do not rule out the impact of spring seepage within the pan and its potential to influence overlying landform processes, we have found little evidence that these landforms in the Makgadikgadi Basin owe their formation to spring activity, as suggested by McFarlane and Long (2015), and therefore are spring mounds. Of the mounds whose sediments were analysed in detail in previous studies (Burrough et al., 2012; Franchi et al., 2020) none contained precipitated evaporites or evidence of surface water seepage. Evidence of seepage from the mound surface, also cited by these authors as evidence for spring flow, is readily explained by runoff from the crusted surfaces during rainfall events. Neither do we find much plausibility in the theory that these mounds were formed through selective erosion of the lake shorelines by shallow streams that created lobate morphologies and eventually

isolated mounds (Franchi et al., 2020). This idea is problematic, in part because there are no identified shorelines that formed during the periods the mounds are dated to (4.9 ± 0.6 ka 1.7 ± 0.1 ka (Burrough and Thomas, 2013) and $0.36 - 0.08$ ka (this study) and in part due to their wide and discontinuous spatial distribution throughout the evaporitic pan surface.

We hypothesise that differential drying of the Pan surface leaves some areas wetter (and 'stickier', cf Fryberger et al., 1988) than others during transitional periods between dry/wet phases driven by either seasonal flooding or longer-term (decadal/centennial) lake regressions. It is not clear what factors cause some areas to dry out faster than others but there is significant variations in sediment grain size, sorting and geochemical precipitation (e.g. silcretes and calcretes) within both surface and subsurface sediments that likely impacts water holding capacity. The location and depth of the Kalahari dyke swarm and neotectonics, may impact moisture at the surface through the influence on topography, subsurface sediments and groundwater flow (Eckardt et al., 2016), but local inflow and direct precipitation also play an important role in the extent and location of groundwater ponding. Differential drying would result in the development of dry surfaces potentially providing sediment for aeolian erosion and downwind transport, and wetter ('stickier') surfaces that hinder the competency of windblown saltation, hence providing a focus for aeolian deposition and mound growth. The importance of surface moisture in dune initiation has been widely acknowledged due to its control on surface erodibility and saltation dynamics, as well as its secondary effect on vegetation growth and competence (Ewing and Kocurek, 2010; Fryberger et al., 1988; Mayaud et al., 2017b; Nield, 2011; Nield and Wiggs, 2011; Rachal and Dugas, 2009), with boundaries between wet and dry areas impacting wind erosion thresholds and saltation efficiency (Nield et al., 2011; Nield and Wiggs, 2011; Wiggs et al., 2004a, 2004b). Given evidence for subsurface moisture beneath the mounds (Franchi et al., 2020), it seems plausible that the interaction

between the changing moisture status of the pan surface and the dynamics of aeolian sediment transport might ultimately lead to the accumulation of sediments and mound formation.

Moist sand surfaces are known to significantly decrease sand flux (Fryberger et al., 1988; Wiggs et al., 2004a) and this can lead to the creation of adhesion structures (small elevated regions of deposited sediment) where dry sand saltates across a moist surface (Davidson-Arnott et al., 2008; Kocurek and Fielder, 1982; Nield et al., 2011). This deposition of dry sand alters saltation dynamics at the dry/wet transition with saltation being less efficient on the deposited dry granular material than the surrounding non-erodible pan surface (Martin and Kok, 2017; Valance et al., 2013). This encourages further sedimentation leading to the growth of sand patches and protodunes (Nield et al., 2011) which may develop into mature dunes. Once sediment has accumulated a few centimeters above the pan floor, it may be stabilised further by the growth of vegetation, the presence of which may also encourage additional sediment deposition (Mayaud et al., 2016, 2017a; Wiggs et al., 1995).

Patterns of dune development have commonly been investigated at the landscape scale (Davidson-Arnott et al., 2008; Long and Sharp, 1964; Mayaud et al., 2017b; Thomas and Wiggs, 2008). This scale of approach allows complex environmental, climatic and landscape interactions to be captured and has frequently been undertaken using a range of methods including cellular automata (CA) modelling (Baas and Nield, 2007; Mayaud et al., 2017a; Nield, 2011; Richards et al., 2020; Rozier and Narteau, 2014) and optically stimulated luminescence (OSL) dating (e.g. Burrough et al., 2012). CA models have been a popular research tool due to the model's ability to spatially capture environmental dynamics at a landscape scale using only fundamental processes, while also being relatively computational efficient compared to other model types, such as computational fluid dynamic models (Mayaud et al., 2017a; Wolfram, 1984). The Vegetation and Sediment TrAnsport (ViSTA) model is a CA model that couples

vegetation and sediment transport processes (Mayaud et al., 2017a). Given the interactions between vegetation dynamics and sediment transport observed in the Ntwetwe Pan, ViSTA provides us with a tool for investigating landscape dynamics and subsequent landform evolution within the Pan. By using OSL dating we can compare the timing and rate of sediment accumulation of the modelled dunes to those found in the pan.

1.4 Research aim

This study explores the viability of the sticky mound hypothesis as a mechanism for dune formation on the Ntwetwe Pan using a numerical model (ViSTA) coupled with OSL dating of mounds in the Ntwetwe Pan. Our goal is to evaluate the potential for uneven drying of the pan surface to drive differential aeolian sediment deposition and crescentic mound growth. We specifically aim to test:

1. The role of moisture patches on the surface of the pan floor as a potential driver of sediment deposition.
2. The dynamics of mound formation, evaluating the modelled dunes' morphologies, and direction and rate of growth in comparison to that derived from OSL dating of a small mound on the eastern margins of Sua Pan.
3. The persistence of established mounds in the landscape in response to changing hydrological dynamics.

2 Methods

2.1 *ViSTA model*

We used the ViSTA model to investigate the role of moisture patches as a potential driver for sediment deposition, dune dynamics, and dune persistence. ViSTA is a coupled cellular automaton numerical model that has been developed as a versatile tool to investigate the development of dryland landscapes in a spatially explicit manner (Mayaud et al., 2017a). It was originally developed to investigate dune stabilisation and reactivation in the Kalahari Desert (Mayaud et al., 2017a, 2017b). It is formed of two interacting modules (sediment transport and vegetation) that resolve interactions and feedbacks between wind flow dynamics, sediment transport and vegetation growth. The sediment transport module determines the amount and direction of sediment movement across the model domain in response to wind characteristics. The vegetation module simulates the growth and survival of vegetation in response to environmental conditions. The model relies on local neighbourhood operations to enable dynamic landscape responses to emerge. More information on the model setup and field data used to parameterise the ViSTA model can be found in Mayaud et al. (2017a).

We developed additional functions within ViSTA to simulate the seasonal flooding and drying processes associated with ephemeral pans (Nield et al., 2015). To capture the seasonal flooding events that occur in the Ntwetwe Pan, the model simulated flooding over a 3-month period with the depth and variability of the flooding determined by the user. During this period, sediment in the flooded area was reworked into a flat surface and any vegetation in the flooded area died. After the flooding period, the erodibility of the flat surface remained low for 3 months to simulate the formation of salt crusts on the pan surface. As cracks in the crust developed, sediment was exposed (Nield et al., 2015) and thus sediment in the model domain was able to be eroded and transported across the model domain. This seasonal

cycle was repeated for the duration of the model run. All model runs in this study represented a period of 100 years in real time (8000 model iterations).

We also developed a function within ViSTA that enabled a zone with high surface moisture to be present within the model domain. In this moist zone, deposition was promoted while erodibility was low (Table 1). Franchi et al. (2020) identified a rising capillary fringe below the sand mounds suggesting the impact of the moisture patch on the given area continues beyond the point at which sediment begins to accumulate at a mound site. The shape/size and longevity of the moisture patch was determined by the user.

2.1.1 Initial conditions

Initial climatic conditions for running the ViSTA model were based on observed 10-minute frequency wind speed (at 6 m height) and wind direction data derived from a meteorological station positioned on nearby Sua Pan (ca. 90 km east of Ntwetwe Pan) during the dry and windy winter season between July and August 2011. For each model iteration, a wind velocity was randomly selected from the observed wind velocity and direction distributions, adjusted depending on vegetation morphology and surface topography, and inputted into the model (Figure 3). Following Mayaud et al. (2017a), the wind erosion threshold for sediment entrainment was set at 5 m s^{-1} and 20 wind events (each lasting 15 hours) were simulated per season. Rainfall was modelled with a mean of 400 mm yr^{-1} reflective of current annual rainfall in the region (Burrough et al., 2012).

The modelled vegetation cover was initially set to zero to reflect areas of newly exposed salt pan. The model's inbuilt dynamic colonisation function enabled vegetation to colonise areas of deposited sediment depending on the spatially explicit environmental stressors. The vegetation simulated within ViSTA was limited to grasses to reflect the dominance of grasses on the pan floor (Burrough et al., 2012).

We parameterised the surface resetting process on the pan by redistributing the sediment in low lying areas (< 0.5 m) and areas impacted by seasonal flood events. This captured the combination of a high water table and flooding events in the Makgadikgadi Basin that result in the seasonal resetting (smoothing) of the pan surface (Nield et al., 2015). While data on the depth of flooding in the Makgadikgadi Basin is limited, by assessing the extent of flooded areas, we inferred that the flooding is relatively shallow (<https://global-surface-water.appspot.com/map>) and maximum flooding levels are thought to be approximately 1 m in depth (Burrough et al., 2012). The depth of flooding was selected from a normal distribution (mean = 0.5 m; standard deviation = 0.4 m). If the selected depth was below 0, it was re-allocated randomly between zero and the mean, resulting in a positively skewed depth distribution.

We used a starting sand depth of 0.5 m distributed across the pan surface, unless otherwise stated, to reflect the sediment limited nature of the Makgadikgadi Pan (Bryant et al., 2007). The influence of greater sediment availability is discussed later in the paper.

The model runs were predominantly undertaken on a 100 by 100 grid, where each grid square represented 1 m. This grid size was chosen as a balance between the area of landscape modelled and computational resources required to run the model. Several larger model runs were undertaken (Table 2) as a proof of concept to show the processes occurring at a larger spatial scale.

The model's sensitivity to the starting wind speed, flooding depth and sediment height were tested (Supporting information, Section 1). The model was robust to these changes, suggesting that even under potential variations in past climates, the model results would still be broadly applicable for variations in mean annual rainfall between 300 - 500 mm, mean flooding depths between 0.3 - 0.7 m and mean

273 annual wind speed of $\pm 1 \text{ m s}^{-1}$ compared to present day speeds (Supporting information, Figures S1, S2
274 and S3).

275 2.1.2 Experimental runs

276 We simulated a range of pan surface conditions to test the efficacy of the sticky mound hypothesis and
277 tested the impact of the following on mound dynamics (Table 2):

- 278 i) the size of the moisture patch;
- 279 ii) the shape of the moisture patch
- 280 iii) the landscape scale represented by the model domain,
- 281 iv) sediment availability; and
- 282 v) the longevity of the moisture patch.

283 Due to the inherent variability in the model (Mayaud et al., 2017a), five model runs were undertaken for
284 each condition.

285 2.1.3 Morphology of modelled mounds

286 Morphometric analysis was applied to the mounds in the model domain at the end of the model run.
287 This analysis has previously been applied to the mounds in the Makgadikgadi basin as a method for
288 distinguishing between subaqueous and aeolian dune formation processes (e.g. Breed and Grow, 1979;
289 Burrough et al., 2012; Long and Sharp, 1964). Two parameters used for dune morphology are the horn-
290 to-horn dune width and the toe-to-brink dune length (e.g. Burrough et al., 2012), with the ratio between
291 being used as a descriptive measures of dune morphometry (Hesp and Hastings, 1998). The horn-to-
292 horn widths and dune lengths of the modelled mounds were calculated using the same methodology as,
293 and compared to, morphometric data previously compiled by Burrough et al. (2012). In addition, the
294 volume of sediment stored within the mounds and the distance between the mound's toe and edge of
295 the moisture patch were calculated.

2.2 OSL Dating of Mound Ridges

To compare the dynamics of modelled mound formation to those occurring on the pan surface, we used OSL dating to establish the last depositional age of the accumulated sediments (Figure 5). We augured three samples from three distinct ridges of a small crescentic mound (Figure 2c), located in Sua Pan on the eastern side of the Makgadikgadi basin.

Samples were taken in opaque plastic tubing and only opened in subdued, long-wavelength (600 nm) light within the laboratory. The unexposed quartz within the tube was isolated using standard quartz isolation techniques (see supporting information). Samples were mounted on either array of a hundred 300- μ m holes in the surface of disc for single grain measurements or directly on to aluminium discs (aliquots) using silica spray and a 2 mm mask.

2.2.1 Equivalent dose (D_e) Determination

Multi-grain preheat plateau and range-finder tests were carried out for a subset of samples. The D_e for each aliquot was measured using a standard single-aliquot regenerative-dose (SAR) protocol (Murray and Wintle, 2003). Full experimental description is provided in supporting information.

2.2.2 Dose Rate (D') Determination

The dose rate for OSL age calculation was determined using Inductively Coupled Plasma Mass Spectrometry (ICP-MS) to measure isotope concentrations (^{232}Th , ^{238}U and ^{40}K) within the sample. Conversion to external beta and gamma components (to account for grain-size, HF etching and moisture content) used the dose-rate conversion and beta attenuation factors of Brennan (2003) and Guérin et al. (2011, 2012), assuming radioactive equilibrium in the ^{238}U and ^{232}Th series. Sample moisture contents

during burial were estimated at 10 ± 5 %. Cosmic-ray dose was calculated according to Prescott and Hutton (1994).

2.2.3 Age Model selection

Single grain ages, where available, were calculated using the central age model (CAM). Multigrain analysis however masks anomalous D_e 's with poor luminescence characteristics and/or residual doses and the inclusion of these grains cause averaging effects to overestimate sample depositional age (Russell and Armitage, 2012). We therefore used the 3-parameter minimum age model (MAM3) to mitigate against this effect and minimise any age overestimates. In its strictest sense the MAM3 model is only really appropriate for use with single grain data (Arnold et al., 2009) but empirical comparison showed greatest convergence between single and multiple grain measurements using this model (Supporting information; Figure S5) suggesting that pragmatically, this model minimised the anomalous impact of age overestimation.

3 Results and discussion

3.1 Methodological approach

The versatility of the ViSTA model combined with OSL dating has enabled us to capture key geomorphic processes associated with mound formation in the Makgadikgadi Pans. Previous research investigating the origins of these mounds have predominantly used field or remote sensing data (Burrough et al., 2012; Franchi et al., 2020; McFarlane and Long, 2015). While these approaches provide important insights into the present and past morphology of the mounds, the approach used in this study has enabled us to investigate and test mound initiation and development processes under multiple environmental conditions while relating it to evidence from real mounds in the pan.

3.2 *Role of moisture patches as a driver of deposition*

Our results show that moisture patches can drive depositional processes. In all model scenarios tested, dune development predominantly occurred on the upwind area of the moisture patch forming a depositional mound on the pan surface (Figure 4; Supporting information, Figure S5-S9). This suggests that on a pan, such as Ntwetwe, the location of residual surface moisture following seasonal flooding or rainfall could act as a key control on the location of dune development over a pan surface where active wind-driven saltation is taking place. The layering of recently deposited sediment over lake bed surfaces was similarly seen within the OSL ages calculated as part of this study which show the mound we sampled was deposited very recently (within the last 400 years) and overlies a much older lake bed (c. 60 ± 5 ka) (Figure 5; Table 3).

3.3 *Mound morphology*

The simulated mounds were found to be morphometrically comparable to mounds previously measured in the Ntwetwe Pan (Burrough et al., 2012). The height of the simulated dunes, which ranged from between 4 m and 7 m, corresponded well to the relatively flat nature of the mounds found in the Ntwetwe Pan that range between 1 m and 10 m tall (Franchi et al., 2020) and, the ratio between the length and width of the modelled mounds fell within the range of the mounds found in the Pan (Figure 6). The width and length of the modelled mounds were, however, smaller than many found in the Pan, due to the spatial scale of the model domain, and lacked the range and variation of length to width ratios seen in the Ntwetwe dunes (Figure 6). This suggests that although the processes within ViSTA capture the key geomorphological processes impacting sediment movement across a pan surface, additional factors not currently included within the model (e.g. variations in surface topography, grain size variability, intra-pan sediment availability), may also influence dune morphology (McFarlane and Long, 2015).

361

362 Results from this study also suggest that the length of the dry/wet boundary perpendicular to the
363 prevailing wind and sediment availability are important controls on the size, shape and volume of the
364 resultant dune (Figure 7) (Nield et al., 2011; Wasson and Hyde, 1983). Boundaries of < 10 m resulted in
365 the formation of an oval shaped dune, while crescentic dunes formed along longer boundaries (Figure
366 4a-d). The openness of the crescentic arch also varied, with more open arches having formed along
367 longer dry/wet boundaries. Increases in the initial starting sand depth (Figure 4k-o) resulted in dunes
368 becoming notably more elongated with greater starting sand depths (Figure 7).

369

370 In contrast to the size of the moisture patch, the morphology of the modelled dunes were broadly
371 insensitive to the shape of the moisture patch (Figure 4e-g; Figure 7), with crescentic dunes of similar
372 sizes forming regardless of whether the moisture patch was square (singular or multiple), rectangular or
373 circular. The lack of sensitivity to the shape of the moisture patch, further highlights the likely
374 importance of the dry/wet boundary (Nield et al., 2011), rather than the surface expression of the
375 moisture patch, in driving the dune formation process. Unlike Nield et al. (2011), who undertook
376 experiments in a beach environment, we find no evidence of erosion at the dry/wet interface. However,
377 this erosion could be masked by the seasonal resetting of the pan surface. Further field monitoring is
378 required to assess the extent to which this occurs in pans such as Ntwetwe.

379

380 We also found notable differences in the length-width ratio between the simulated mounds to other
381 lake bed dunes in Australia and Africa (Burrough et al., 2012; Franchi et al., 2020). The simulated
382 mounds had a significantly smaller length to width ratio compared to dunes found in Lake Chad (t-test, p
383 <0.05 , $df = 71$), Australia's Lakes Amadeus and Mackay (t-test, $p <0.05$, $df = 67$), and known subaqueous
384 dunes (t-test, $p <0.05$, $df = 160$) (Burrough et al., 2012). Without ground-truthing in these systems, it is

hard to extrapolate the findings here to imply other lake-bed dunes were formed in a similar way. However, in many of these lake systems, there is evidence of periodic wetting and drying as well as readily available aeolian sediments moving across the lake floor, suggesting the sticky mound hypothesis may be a viable mechanism for building the dune forms identified in Figure 1a-e. Local environmental conditions (e.g. variability in wind direction, sediment supply and surface topography) are likely to be important in determining the specific dune shape/size in each system.

The range of simulated mound shapes, including oval, crescentic and more sinuous dune shapes, reflected the variety of mound shapes seen in the Ntwetwe Pan (Figure 8). In the Ntwetwe Pan more compound and sinuous dunes are located in the western region of the pan. Our findings suggest that these more sinuous dunes could form in response to conditions with greater sediment supply than the eastern region, perhaps purely from its cumulative downwind location. However, Burrough and Thomas (2013) noted that OSL ages from mounds from the western region of the basin tend to be older in age (4.9 - 4.4 ka) than those in the east (3.4 - 1.7 ka). This, in conjunction with our findings, may indicate several periods of dune formation, with earlier periods of dune building perhaps occurring under conditions of greater sediment supply/availability resulting in more compound forms in their morphology.

3.4 Mound dynamics

Sediment accumulation occurred on the modelled moisture patch over the full duration of the model run (Figure 9a-d). Vegetation rapidly colonised areas of sediment accumulation, promoting further deposition and reducing sediment erosion (Leenders et al., 2007; Mayaud et al., 2016), resulting in mound stabilisation (Mayaud et al., 2017b; Wiggs et al., 1995). Similar patterns of sediment accumulation were seen in the OSL data with ridge ages suggesting that sediments on the mound

sampled in the Ntwetwe Pan have accumulated over time both vertically and laterally (Table 3). The lack of subsequent downwind migration of deposited sediment further into the moisture patch supports findings by Franchi et al. (2020), whose geophysical investigations of the Ntwetwe mounds showed that, whatever the formative mechanism, moisture was drawn towards the surface of the dunes via capillary action, making the mounds less susceptible to erosion.

Results from the model also showed mound growth in an upwind direction away from the dry/wet boundary of the moisture patch (Figure 10). In contrast to barchan dunes, where we would expect the youngest sediment to be found on the leeside of the dune, the simulated dunes within ViSTA presented younger sediment accumulations on the upwind slope of the mound. This corresponds with the OSL dating of concentric terraces on the mounds in the Makgadikgadi basin (Table 3, Figure 5) which indicate that the inner ridge (SUA/15/8; 360 ± 40 and 220 ± 30 years ago) is distinctly older than the outer ridge (SUA/15/7; 130 ± 13 and 80 ± 10 years ago). This suggests that the increased deposition caused by uneven drying of the pan surface could drive an adverse pressure gradient, with windward slope steepness reaching up to 30 degrees on some mounds, slowing the wind speed upwind of the mound and increasing rates of deposition here.

The rate of upwind mound growth occurred most rapidly ($\sim 0.1 - 0.4 \text{ m yr}^{-1}$) over the first quarter of the model simulation (25 years) before stabilising. The OSL data suggests sediments accumulate discontinuously at rates of between 0.4 and 2.9 cm yr^{-1} building upwards and then upwind on timescales of centuries to decades. Such differences in the modelled and OSL growth rates could be caused by variable sediment fluxes not captured by the model. The model did not capture the distinctive terracing seen on the mounds in the Makgadikgadi basin (Figure 2a) likely due to the difference in timescale of formation. OSL data suggests the terracing, related to phases of concentric outward dune building,

occur over multiple decades (i.e. 360-220; 210-160; 130-80 yrs), a timescale not inconsistent with the 60-120 year variability identified in southern African climate records from tree ring and isotope data (Tyson et al., 2002).

3.5 Persistence of mounds

In all tested model scenarios, the persistence of the mounds in the model landscape was found to be dependent on the longevity of the moisture patch (Figure 4 and Figure 9). When the moisture patch remained constant in time and space, the presence of a dune feature on the moisture patch remained constant with the mound shape being dependent on the sediment flux across the model domain (Figure 4p; Supporting information Figure S9, S10). During periods of low sediment flux, the dune feature was seen to be eroded into a more rounded morphology. Then, when the sediment store was replenished, such as when the path of a transient dune crosses the location of the moisture patch, a crescentic shape evolved. This cycle of degradation and re-forming was found to occur multiple times over a centennial time period and can be seen in Figure 10e ('Continuous' and 'Gradual Loss') where the distance of the mound upwind of the dry/wet boundary fluctuates over time in response to the sediment availability.

In the model simulations where the wetness of the moisture patch decreased over time (Figure 4q and r), sediment erodibility was seen to increase coupled with the loss of vegetation. As a result, the mound lost its crescentic shape, becoming more oblong and perpendicular to the prevailing wind, before becoming reactivated and migrating downwind. This reactivation process resulted in a complete loss of sediment stored in stabilised mound formations on the moisture patch (Figure 9e). In Ntwetwe Pan, ground-truthing has revealed that dune footprints similarly have little observable topographic expression (Burrough et al., 2018) but are also characterised by increased cohesion or hardness of sediments and/or a surface lag of granules (Figure 2b). This residual cohesive 'footprint' may be caused

455 both by diagenetic processes occurring at the mound/lakebed interface, particularly related to the
456 mobilization of silica as moisture levels fluctuate, and/or to larger residual particles from the mound
457 remaining in place after the finer, more erodible sediments have been winnowed out. The limits of the
458 model, do not allow us to capture the increased cohesion of the mound 'footprints' nor assess to what
459 degree vegetation responds to changes in moisture availability as it is possible that deeper groundwater
460 supplies could support vegetation, minimising rates of dune reactivation. Further work should now be
461 undertaken to investigate these interactions.

462

463 Regarding the dissipation of the mounds, the key finding of this study is that, unlike the interpretation of
464 Burrough and Thomas (2013), who assumed a migratory barchan model for the landforms, we have
465 found that the dunes are more Nebkha-like in form reactivating and dispersing downwind. This has
466 implications for interpreting past environments. Interpreted as barchans, Burrough and Thomas (2013)
467 inferred that OSL dates from the dunes represented the transition from dry conditions to wet conditions
468 as dunes stopped migrating due to increased moisture and vegetation colonisation. As there is no
469 evidence of mobile dunes under present day conditions, it was thought that such dry periods must have
470 been more arid than today. If the formative mechanism of dune formation (and dissipation) tested in
471 the model here is correct, OSL ages may represent environments not unlike today, where the lake bed
472 seasonally transitions from wet conditions to dry conditions with residual moisture patches, allowing
473 these sticky surface patches to rapidly accumulate into distinct landforms. As such, the mounds may be
474 initiated in response to a drying phase. In the Ntwetwe pan, the uneven spatial distribution of the
475 mounds, with more mounds found on the western side of the pan, is likely a result of the predominantly
476 westward direction of sediment transport but could also suggest that residual moisture patches could
477 have formed in the area, promoting sediment accumulation processes. The implications of this
478 difference in interpretation could potentially be very important to the palaeoenvironmental research

community in the Kalahari region and other dryland zones where landforms (geoproxies) dominate the record of past climate change (Thomas and Burrough, 2013).

If the Makgadikgadi dunes can be used as possible analogues for reconstructing the palaeo-landscape of Martian equatorial layered deposits, as suggested by Franchi et al. (2020), then the findings from this study suggest differential drying of the Martian surface could provide one explanation for similar forms observed there (Pondrelli et al., 2015), or at least a similar mechanism of preservation through the interaction with moisture. Further research investigating the role of differential drying on dune formation is certainly warranted. A combination of field work and remote sensing data could be used to identify areas within former lake beds where dry/wet boundaries have newly formed. These areas could be monitored for dune initiation processes. Coupled with further parameterisation of the ViSTA model, this would enable complex interactions between moisture and sediment transport processes to be captured and at a higher resolution.

4 Conclusion

Following a suite of inconclusive investigations into the formative mechanisms of crescentic lake bed mounds in the Makgadikgadi basin, we propose and test the “sticky mound hypothesis” as a potential formative process. This theory posits that uneven surface moisture on the pan floor can drive the formation of the mounds by increasing deposition in the moist area causing a mound feature to form.

We use a computational model, ViSTA, coupled with OSL dating of a mound from the Makgadikgadi Basin to test this theory. We found that crescentic mounds formed when moisture was present on the pan surface, with sediment deposition predominantly occurring on the upwind edge of the moisture patch. The simulated mounds were also found to grow in an upwind direction, onto the dry pan surface

502 corresponding with the OSL data showing the youngest sediments are found on the upwind edge of the
503 mound. The loss of wetness on the moisture patch resulted in the model dunes mobilising and
504 dispersing down wind. Therefore, these results suggest that the location of residual surface moisture
505 following seasonal flooding or rainfall could act as a key control on the location of dune development.
506 These findings raise questions about the paleoenvironmental history of the area, suggesting that
507 mounds could have formed under similar conditions to those seen today – not more arid conditions as
508 previously suggested.

509 **Data availability statement**

510 Data are available on reasonable request from the authors.

511 **Funding statement**

512 SLB acknowledges funding from the Trapnell fund and National Geographic.

513 **Acknowledgements**

514 Fieldwork was carried out under permit EWT 8/36/4 xxx (60) issued by the Ministry of Environment,
515 Wildlife and Tourism, Botswana to Dr SL Burrough. Meteorological data were provided by the DO4 field
516 team (Natural Environment Research Council grant NE/H021841/1; Botswana Ministry of Environment,
517 Wildlife and Tourism research permit no. EWT 8/36/4 XIV) and we acknowledge the support of
518 Botswana Ash (Pty) Ltd.

519

520 The authors have no conflicts of interest to declare.

Author contributions

SB and TH conceived of the project with SB and JR developing the approach. JR and SB developed and ran the model with data collected by GW. SB, DT and MM conducted field investigations that generated the samples analysed in this paper. SB calculated the luminescence dates. JR, SB and GW wrote the paper. JR, SB, GW, DT and TH contributed to editing. All authors read and approved the final version of the manuscript.

References

- Armitage SJ, Bristow, CS, Drake, NA, 2015. West African Monsoon dynamics inferred from abrupt fluctuations of Lake Mega-Chad. PNAS 112, 28, 8543-8548. DOI: [10.1073/pnas.1417655112](https://doi.org/10.1073/pnas.1417655112)
- Arnold LJ, Roberts RG, Galbraith RF, DeLong SB. 2009. A revised burial dose estimation procedure for optical dating of young and modern-age sediments. Quaternary Geochronology **4** : 306–325. DOI: 10.1016/j.quageo.2009.02.017
- Baas ACW, Nield JM. 2007. Modelling vegetated dune landscapes. Geophysical Research Letters **34** : L06405. DOI: 10.1029/2006GL029152
- Bourke MC, Goudie AS. 2009. Varieties of barchan form in the Namib Desert and on Mars. Aeolian Research **1** : 45–54. DOI: 10.1016/j.aeolia.2009.05.002
- Breed CS, Grow T. 1979. Morphology and distribution of dunes in sand seas observed by remote sensing. US Geological Survey, Professional Paper **1052** : 253–302.
- Brennan BJ. 2003. Beta doses to spherical grains. Radiation Measurements **37** : 299–303. DOI: 10.1016/S1350-4487(03)00011-8
- Bristow CS, Drake N, Armitage S. 2009. Deflation in the dustiest place on Earth: The Bodélé Depression,

542 Chad. *Geomorphology* **105** : 50–58. DOI: 10.1016/j.geomorph.2007.12.014

543 Bryant RG, Bigg GR, Mahowald NM, Eckardt FD, Ross SG. 2007. Dust emission response to climate in
544 southern Africa. *Journal of Geophysical Research* **112** : D09207. DOI: 10.1029/2005JD007025

545 Burrough S, Thomas D, Staurset S, Allin J, Nash D, Coulson S, Mothulatshipi S. 2018. Salt, mud and
546 stones: Unpicking archaeological landscapes in the southern African interior [online] Available from:
547 <https://meetingorganizer.copernicus.org/EGU2018/EGU2018-14962.pdf>

548 Burrough SL, Thomas DSG. 2013. Central southern Africa at the time of the African Humid Period: A new
549 analysis of Holocene palaeoenvironmental and palaeoclimate data. *Quaternary Science Reviews* **80** : 29–
550 46. DOI: 10.1016/j.quascirev.2013.08.001

551 Burrough SL, Thomas DSG, Bailey RM. 2009. Mega-Lake in the Kalahari: A Late Pleistocene record of the
552 Palaeolake Makgadikgadi system. *Quaternary Science Reviews* **28** : 1392–1411. DOI:
553 10.1016/j.quascirev.2009.02.007

554 Burrough SL, Thomas DSG, Bailey RM, Davies L. 2012. From landform to process: Morphology and
555 formation of lake-bed barchan dunes, Makgadikgadi, Botswana. *Geomorphology* **161–162** : 1–14. DOI:
556 10.1016/j.geomorph.2012.03.027

557 Cooke HJ. 1980. Landform evolution in the context of climatic change and neo- tectonism in the middle
558 Kalahari of north-central Botswana. *Transactions, Institute of British Geographers* **5** : 80–99. DOI:
559 10.2307/622100

560 Davidson-Arnott RGD, Yang Y, Ollerhead J, Hesp PA, Walker IJ. 2008. The effects of surface moisture on
561 aeolian sediment transport threshold and mass flux on a beach. *Earth Surface Processes and Landforms*
562 **33** : 55–74. DOI: 10.1002/esp.1527

563 Eckardt FD, Bryant RG, McCulloch G, Spiro B, Wood WW. 2008. The hydrochemistry of a semi-arid pan

564 basin case study: Sua Pan, Makgadikgadi, Botswana. *Applied Geochemistry* **23** : 1563–1580. DOI:
 565 10.1016/j.apgeochem.2007.12.033

566 Eckardt FD, Cotterill FPD, Flügel TJ, Kahle B, McFarlane M, Rowe C. 2016. Mapping the surface
 567 geomorphology of the Makgadikgadi Rift Zone (MRZ). *Quaternary International* **404** : 115–120. DOI:
 568 10.1016/j.quaint.2015.09.002

569 Elburg M, Goldberg A. 2000. Age and geochemistry of Karoo dolerite dykes from northeast Botswana.
 570 *Journal of African Earth Sciences* **31** : 539–554. DOI: 10.1016/S0899-5362(00)80006-8

571 Ewing RC, Kocurek GA. 2010. Aeolian dune interactions and dune-field pattern formation: White Sands
 572 Dune Field, New Mexico. *Sedimentology* **57** : 1199–1219. DOI: 10.1111/j.1365-3091.2009.01143.x

573 Franchi F, MacKay R, Selepeng AT, Barbieri R. 2020. Layered mound, inverted channels and polygonal
 574 fractures from the Makgadikgadi pan (Botswana): Possible analogues for Martian aqueous
 575 morphologies. *Planetary and Space Science* **192** : 105048. DOI: 10.1016/j.pss.2020.105048

576 Franchi F, Rossi AP, Pondrelli M, Cavalazzi B. 2014. Geometry, stratigraphy and evidences for fluid
 577 expulsion within Crommelin crater deposits, Arabia Terra, Mars. *Planetary and Space Science* **92** : 34–48.
 578 DOI: 10.1016/j.pss.2013.12.013

579 Fryberger SG, Schenk CJ, Krystinik LF. 1988. Stokes surfaces and the effects of near-surface
 580 groundwater-table on Aeolian deposition. *Sedimentology* **35** : 21–41. DOI: 10.1111/j.1365-
 581 3091.1988.tb00903.x

582 Goudie A, Thomas DSG. 1986. Lunette dunes in southern Africa. *Journal of Arid Environments* **10** : 1–12.
 583 DOI: 10.1016/s0140-1963(18)31260-6

584 Grove, A. T., and Warren, A. 1968. Quaternary landforms and climate on the south side of the Sahara.
 585 *The Geographical Journal* 134: 194-208.

586 Grey DRC, Cooke HJ. 1977. Some problems in the quaternary evolution of the landforms of northern
 587 Botswana. *Catena* **4** : 123–133. DOI: 10.1016/0341-8162(77)90014-5

588 Grove AT. 1969. Landforms and Climatic Change in the Kalahari and Ngamiland. *The Geographical*
 589 *Journal* **135** : 191. DOI: 10.2307/1796824

590 Guérin G, Mercier N, Adamiec G. 2011. Dose rate conversion factors: update. *Ancient TL* **29** : 5–8.

591 Guérin G, Mercier N, Nathan R, Adamiec G, Lefrais Y. 2012. On the use of the infinite matrix assumption
 592 and associated concepts: A critical review. *Radiation Measurements* **47** : 778–785. DOI:
 593 10.1016/j.radmeas.2012.04.004

594 Hesp PA, Hastings K. 1998. Width, height and slope relationships and aerodynamic maintenance of
 595 barchans. *Geomorphology* **22** : 193–204. DOI: 10.1016/S0169-555X(97)00070-6

596 Kocurek G, Fielder G. 1982. Adhesion structures. *Journal of Sedimentary Petrology* **52** : 1229–1241. DOI:
 597 10.1306/212f8102-2b24-11d7-8648000102c1865d

598 Lancaster IN. 1978. The Pans of the Southern Kalahari, Botswana. *The Geographical Journal* **144** : 81.
 599 DOI: 10.2307/634651

600 Leenders JKK, Boxel JH van, Sterk G, van Boxel JH, Sterk G. 2007. The Effect of Single Vegetation
 601 Elements on Wind Speed and Sediment Transport in the Sahelian Zone of Burkina Faso. *Earth Surface*
 602 *Processes and Landforms* **32** : 1454–1474. DOI: 10.1002/esp

603 Long JT, Sharp RP. 1964. Barchan-dune movement in Imperial Valley, California. *Bulletin of the*
 604 *Geological Society of America* **75** : 149–156. DOI: 10.1130/0016-7606(1964)75[149:BMIIVC]2.0.CO;2

605 Martin RL, Kok JF. 2017. Wind-invariant saltation heights imply linear scaling of aeolian saltation flux
 606 with shear stress. *Science Advances* **3** : e1602569. DOI: 10.1126/sciadv.1602569

607 Mayaud JR, Bailey RM, Wiggs GFS. 2017a. A coupled vegetation/sediment transport model for dryland

608 environments. *Journal of Geophysical Research: Earth Surface* **122** : 875–900. DOI:
 609 10.1002/2016JF004096

610 Mayaud JR, Bailey RM, Wiggs GFS. 2017b. Modelled responses of the Kalahari Desert to 21st century
 611 climate and land use change. *Nature: Scientific Reports* **7** : 3887. DOI: 10.1038/s41598-017-04341-0

612 Mayaud JR, Wiggs GFS, Bailey RM. 2016. Dynamics of skimming flow in the wake of a vegetation patch.
 613 *Aeolian Research* **22** : 141–151. DOI: 10.1016/j.aeolia.2016.08.001

614 McFarlane MJ, Long CW. 2015. Pan floor “barchan” mounds, Ntwetwe Pan, Makgadikgadi, Botswana:
 615 Their origin and palaeoclimatic implications. *Quaternary International* **372** : 108–119. DOI:
 616 10.1016/j.quaint.2014.10.008

617 Murray AS, Wintle AG. 2003. The single aliquot regenerative dose protocol: Potential for improvements
 618 in reliability. *Radiation Measurements* **37** : 377–381. DOI: 10.1016/S1350-4487(03)00053-2

619 Nield JM. 2011. Surface moisture-induced feedback in aeolian environments. *Geology* **39** : 915–918.
 620 DOI: 10.1130/G32151.1

621 Nield JM, Bryant RG, Wiggs GFS, King J, Thomas DSG, Eckardt FD, Washington R. 2015. The dynamism of
 622 salt crust patterns on playas. *Geology* **43** : 31–34. DOI: 10.1130/G36175.1

623 Nield JM, Wiggs GFS. 2011. The application of terrestrial laser scanning to aeolian saltation cloud
 624 measurement and its response to changing surface moisture. *Earth Surface Processes and Landforms* **36**
 625 : 273–278. DOI: 10.1002/esp.2102

626 Nield JM, Wiggs GFS, Squirrell RS. 2011. Aeolian sand strip mobility and protodune development on a
 627 drying beach: examining surface moisture and surface roughness patterns measured by terrestrial laser
 628 scanning. *Earth Surface Processes and Landforms* **36** : 513–522. DOI: 10.1002/esp.2071

629 Pondrelli M, Rossi AP, Le Deit L, Fueten F, van Gasselt S, Glamoclija M, Cavalazzi B, Hauber E, Franchi F,

630 Pozzobon R. 2015. Equatorial layered deposits in Arabia Terra, Mars: Facies and process variability.
631 Bulletin of the Geological Society of America **127** : 1064–1089. DOI: 10.1130/B31225.1

632 Pondrelli M, Rossi AP, Le Deit L, Schmidt G, Pozzobon R, Hauber E, Salese F. 2019. Groundwater Control
633 and Process Variability on the Equatorial Layered Deposits of Kotido Crater, Mars. Journal of Geophysical
634 Research: Planets **124** : 779–800. DOI: 10.1029/2018JE005656

635 Pozzobon R, Mazzarini F, Massironi M, Rossi AP, Pondrelli M, Cremonese G, Marinangeli L. 2019. Fluids
636 mobilization in Arabia Terra, Mars: Depth of pressurized reservoir from mounds self-similar clustering.
637 Icarus **321** : 938–959. DOI: 10.1016/j.icarus.2018.12.023

638 Prescott JR, Hutton JT. 1994. Cosmic ray contributions to dose rates for luminescence and ESR dating:
639 Large depths and long-term time variations. Radiation Measurements **23** : 497–500. DOI: 10.1016/1350-
640 4487(94)90086-8

641 Rachal DM, Dugas DP. 2009. Historical dune pattern dynamics: White Sands Dune Field, New Mexico.
642 Physical Geography **30** : 64–78. DOI: 10.2747/0272-3646.30.1.64

643 Richards J, Mayaud J, Zhan H, Wu F, Bailey R, Viles H. 2020. Modelling the risk of deterioration at
644 earthen heritage sites in drylands. Earth Surface Processes and Landforms **45** : 2401–2416. DOI:
645 10.1002/esp.4887

646 Rozier O, Narteau C. 2014. A real-space cellular automaton laboratory. Earth Surface Processes and
647 Landforms **39** : 98–109. DOI: 10.1002/esp.3479

648 Russell NJ, Armitage SJ. 2012. A comparison of single-grain and small aliquot dating of fine sand from
649 Cyrenaica, northern Libya. Quaternary Geochronology **10** : 62–67. DOI: 10.1016/j.quageo.2012.03.005

650 Thomas DSG, Shaw PA. 1991. The Kalahari Environment . Cambridge University Press: Cambridge

651 Thomas DSG, Wiggs GFS. 2008. Aeolian system response to global change: Challenges of scale, process

652 and temporal integration. *Earth Surface Processes and Landforms* **33** : 1396–1418. DOI:
 653 10.1002/esp.1719

654 Tyson PD, Cooper GRJ, McCarthy TS. 2002. Millennial to multi-decadal variability in the climate of
 655 southern Africa. *International Journal of Climatology* **22** : 1105–1117. DOI: 10.1002/joc.787

656 Valance A, Ho TD, Moctar AO El, Dupont P. 2013. Scaling laws in aeolian sand transport: Erodible versus
 657 non-erodible bed. 1059–1062 pp. 18 June

658 Wasson RJ, Hyde R. 1983. Factors determining desert dune type. *Nature* **304** : 337–339. DOI:
 659 10.1038/304337a0

660 Wiggs GF., Baird A., Atherton R. 2004a. The dynamic effects of moisture on the entrainment and
 661 transport of sand by wind. *Geomorphology* **59** : 13–30. DOI: 10.1016/j.geomorph.2003.09.002

662 Wiggs GFS, Atherton RJ, Baird AJ. 2004b. Thresholds of aeolian sand transport: establishing suitable
 663 values. *Sedimentology* **51** : 95–108. DOI: 10.1046/j.1365-3091.2003.00613.x

664 Wiggs GFS, Thomas DSG, Bullard JE, Livingstone I. 1995. Dune mobility and vegetation cover in the
 665 Southwest Kalahari desert. *Earth Surface Processes and Landforms* **20** DOI: 10.1002/esp.3290200604

666 Wolfram S. 1984. Cellular automata as models of complexity. *Nature* **311** DOI: 10.1038/311419a0

667 **Figure Captions**

668 Figure 1: Unidentified concentric landforms on a selection of dry lake beds within the subtropical desert
 669 belts. Inset rectangles are shown at smaller scale below images A, B, C, D as a, b, c and d. A) Lake
 670 MacKay, Northern Territory, Australia, B) Lake Amadeus, Northern Territory, Australia; C) Lake Chad,
 671 North Africa; D) Palaeolake Makgadikgadi, Botswana, E) Etosha Pan, Namibia, Southern Africa; F) Mound
 672 field in the southeastern sector of the Firsoff crater, Mars (Hirise ESP_020679_1820). Images modified
 673 from Burrough et al., 2012; Franchi et al., 2014, 2020.

674

675 Figure 2: a) Crescentic Ntwetwe pan mounds; b) mound 'footprints visible in pan surface sediments
676 (CNES/Airbus Imaged 2016 accessible via Google Earth 2021); c) Drone image of 'island' showing
677 concentric ridging within mound (R20) on Sua Pan. Inset shows location of a, b and c.

678

679 Figure 3: Wind roses for measured data on Sua pan and simulated in the ViSTA model.

680

681 Figure 4: Simulated dune morphologies (aerial view) when the model was initiated with conditions
682 outlined in Table 2. The location of the moisture patch is outlined in white. The model was run using
683 climatic conditions reflective of those found in the Makgadikgadi Basin and for a model equivalent of
684 100 years.

685

686 Figure 5: Cross-section of sand mound with OSL ages shown for each sampled ridge dune R20, shown in
687 Figure 2a and c.

688

689 Figure 6: The length to width ratios of the simulated dunes (red) compared to African (blue), Australian
690 (orange) and subaqueous dunes (green). Data for the non-modelled dunes were originally compiled by
691 Burrough et al. (2012).

692

693 Figure 7: Simulated dune characteristics after a model run equivalent to 100 years. a) Dune width and
694 length; b) Volume of sediment stored in dunes (total) and on the moisture patch (moist patch); c)
695 proportion of dune sediment stored on the moisture patch compared to the total volume of sediment
696 stored in dunes; and d) the total number of dunes in the model domain.

697

Figure 8: Comparison of dunes in the Ntwetwe Pan with model outputs. The central image shows the locations of panels A to F within the Ntwetwe pan. Modelled dunes formed under the following conditions in each panel: a) 6 x 6 m moisture patches; b) 10 x 10 m moisture patches; c) 20 x 20 m, 30 x 30 m and two squares moisture patches; d) 0.7 m starting sand height; e) 0.9 m and 1.1 m starting sand height; and f) 1.3 m starting sand height. All model domains were set at 100 x 100 m. Image Credit: Google Earth, accessed 2021.

Figure 9: Time series of sediment volume (m^3) stored in simulated mound features. The shaded areas indicate one standard deviation from the mean.

Figure 10: Timeseries of mound development upwind from the moisture patch. a) The mean distance of mound formation upwind from the dry/wet boundary (m). b) The mean rate of sediment accumulation upwind from the dry/wet boundary (m yr^{-1}). The shaded areas indicate one standard deviation from the mean.

Tables

Table 1: The erosional and depositional probabilities associated with surface types. Probabilities are based on Mayaud et al., (2017a).

Surface type	Probability of:	
	Erosion	Deposition
Pan surface	0	0.4
Dry sand	0.7-1	0.7
Damp sand	0.2-0.7	0.3
Wet sand	0.2-1	1

719 *Table 2: Model conditions simulated. Conditions with a '*' indicate set up conditions used in this study as a reference.*

Experiment	Conditions tested	Details
Size of moisture patch (square)	2 x 2 m	Moisture patch located centrally in the model domain
	6 x 6 m	
	10 x 10 m*	
	20 x 20 m	
Shape of moisture patch	Square*	10 x 10 m moisture patch located centrally in model domain
	Rectangle	20 x 5 m moisture patch located centrally in model domain, perpendicular to the prevailing wind
	'Circle'	A 20 m diameter moisture patch located centrally in the model domain
	Two Squares	Two 10 x 10 m moisture patches located centrally in model domain, perpendicular to the prevailing wind
Landscape size	100 x 100 m model domain; 10 x 10 m moisture patch*	Square moisture patch located centrally in the model domain
	200 x 200 m model domain; 20 x 20 m moisture patch	
	300 x 300 m model domain; 30 x 30 m moisture patch	
	500 x 500 m model domain; 50 x 50 m moisture patch	
Sediment availability - initial starting sand height	0.3 m	Moisture patch located centrally in the model domain with varying initial sediment heights
	0.5 m*	
	0.7 m	
	0.9 m	
	1.1 m	
	1.3 m	
Longevity of moisture patch presence	Continual moisture patch	Moisture patch remains permanent through whole model run. Starting sand heights were generated by running the model for 100 years under conditions reflective of those in the Makgadikgadi Basin.
	Gradual loss of moisture patch	The wetness of moisture patch linearly decreases over model run. Starting sand heights were generated by running the model for 100 years under conditions reflective of those in the Makgadikgadi Basin.

Sudden loss of moisture
patch

Moisture patch is removed at start of model run. Starting sand heights were generated by running the model for 100 years under conditions reflective of those in the Makgadikgadi Basin.

720

721 *Table 3: OSL age data for samples taken from mound ridges: SUA/15/7, SUA/15/8 and SUA/15/9*

Sample ID	Depth (m)	Grain size dated (μm)	Age Model	n	Overdispersion (%)	De (Gy)	K* (%)	Th* (ppm)	U* (ppm)	Cosmic Dose (Gy/ka)	Total Dose Rate (Gy/ka)	Age (years)
SUA/15/8/1	0.5	180-210	MG MAM	46	5.1 \pm 3.6	0.293 \pm 0.005	0.421	6.781	1.506	0.226	1.32 \pm 0.15	221 \pm 25
SUA/15/8/2	1.0	180-210	MG MAM	49	53.5 \pm 5.6	0.339 \pm 0.019	0.564	4.841	1.301	0.212	1.27 \pm 0.15	267 \pm 34
		180-210	SG CAM	65	Na	0.23 \pm 0.06						190 \pm 50
SUA/15/8/3	1.4	180-210	MG MAM	52	23.8 \pm 3.0	0.357 \pm 0.015	0.326	4.230	1.137	0.202	0.98 \pm 0.11	364 \pm 42
SUA/15/9/1	0.5	180-210	MG MAM	36	Na	0.196 \pm 0.010	0.472	4.918	1.245	0.226	1.20 \pm 0.13	164 \pm 20
		180-210	SG CAM	65	Na	0.12 \pm 0.03						100 \pm 30
SUA/15/9/2	1.0	180-210	MG MAM	42	41.6 \pm 5.0	0.228 \pm 0.014	0.320	4.532	1.156	0.212	1.01 \pm 0.11	225 \pm 28
SUA/15/9/3	1.3	180-210	MG MAM	46	43.7 \pm 4.9	0.297 \pm 0.018	0.630	5.549	1.414	0.205	1.39 \pm 0.16	214 \pm 28
		180-210	SG CAM	65	Na	0.29 \pm 0.05						210 \pm 40
SUA/15/7/1	0.5	180-210	MG MAM	33	36.8 \pm 6.2	0.092 \pm 0.008	0.461	4.614	1.208	0.226	1.16 \pm 0.13	80 \pm 11
SUA/15/7/2	1.0	180-210	MG MAM	42	30.0 \pm 4.6	0.109 \pm 0.014	0.456	4.537	1.165	0.212	1.13 \pm 0.13	97 \pm 16

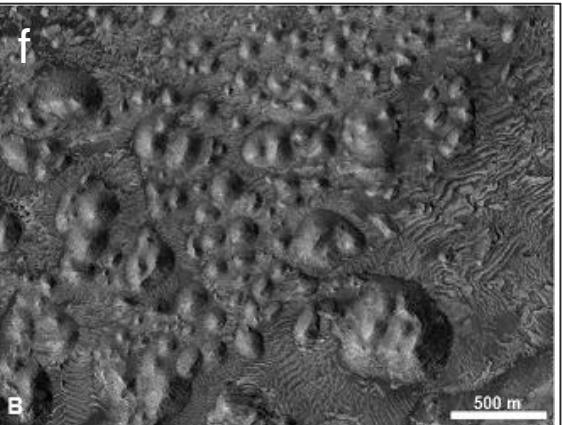
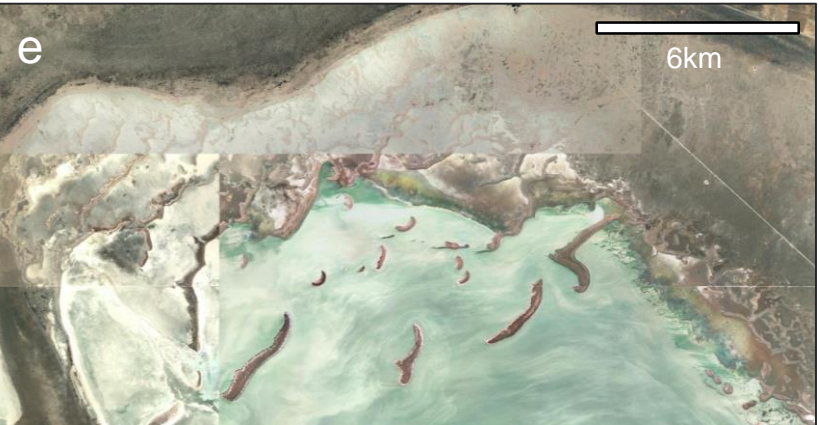
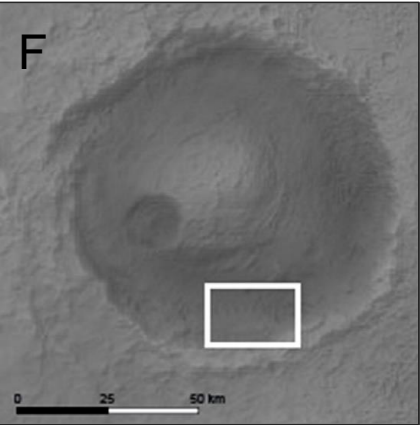
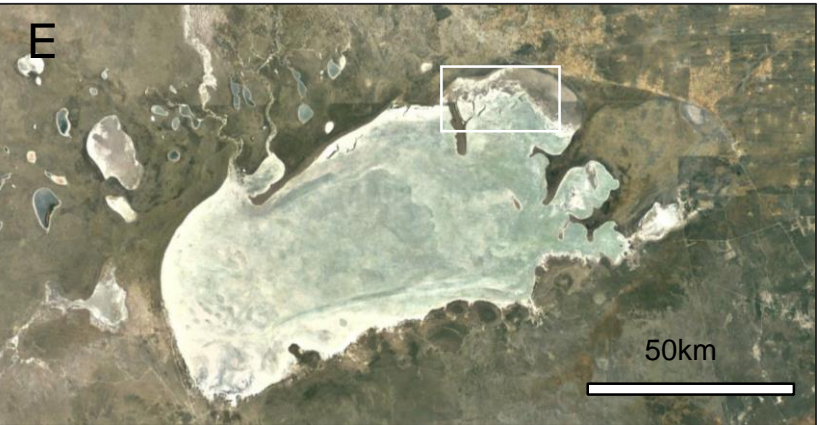
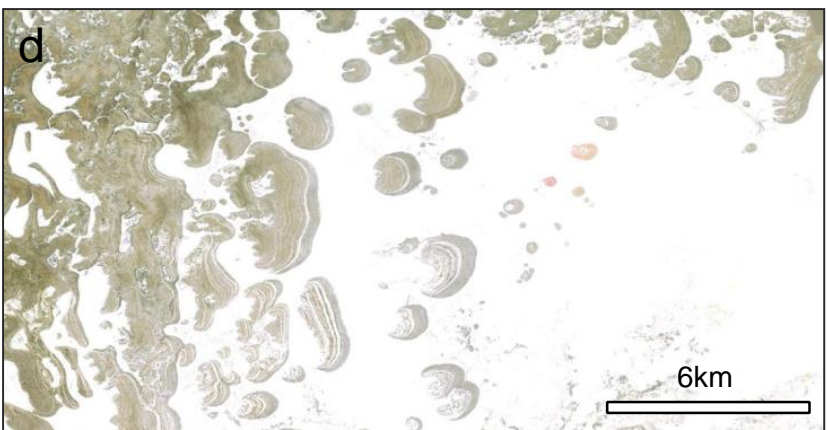
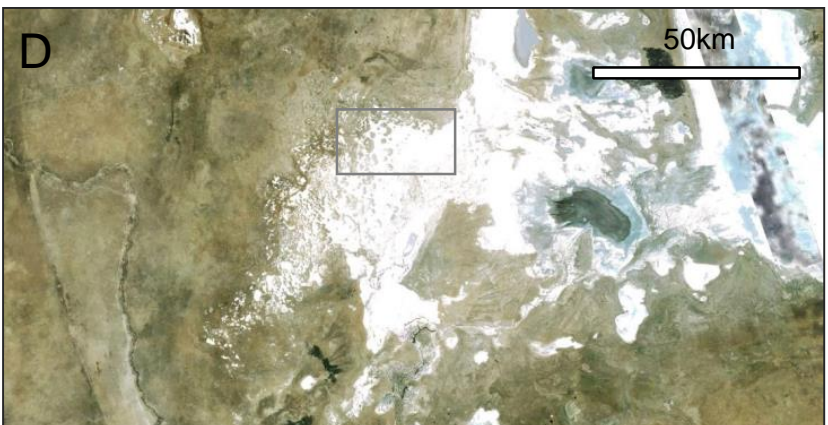
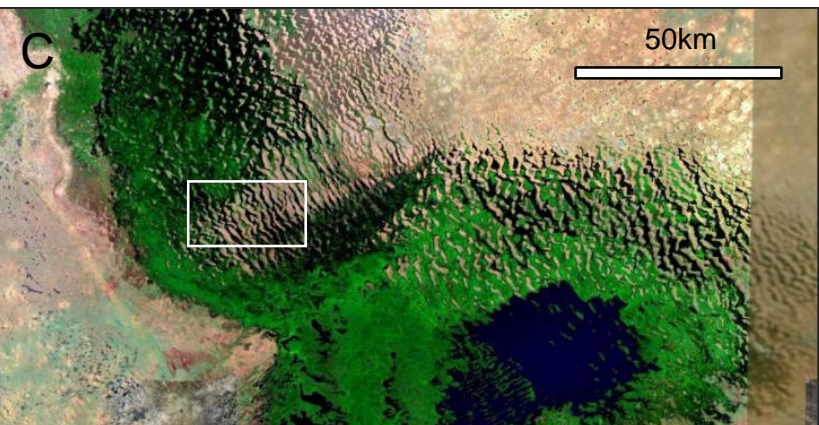
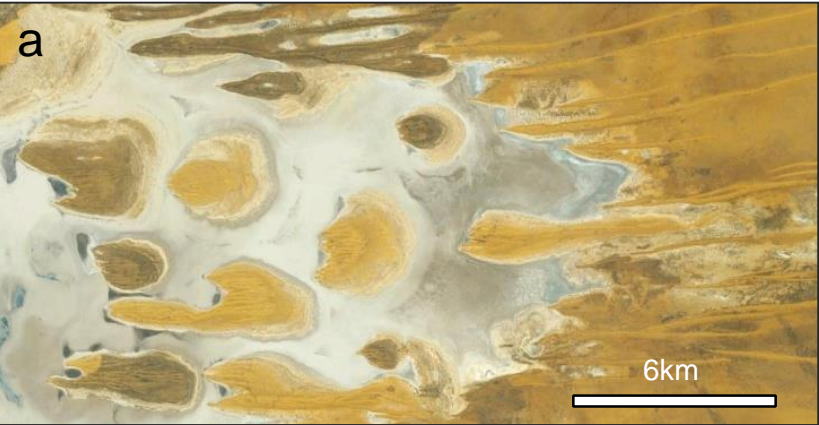
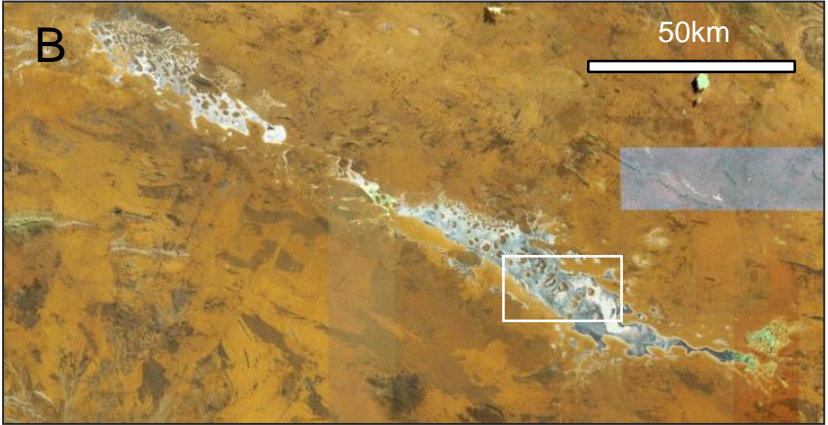
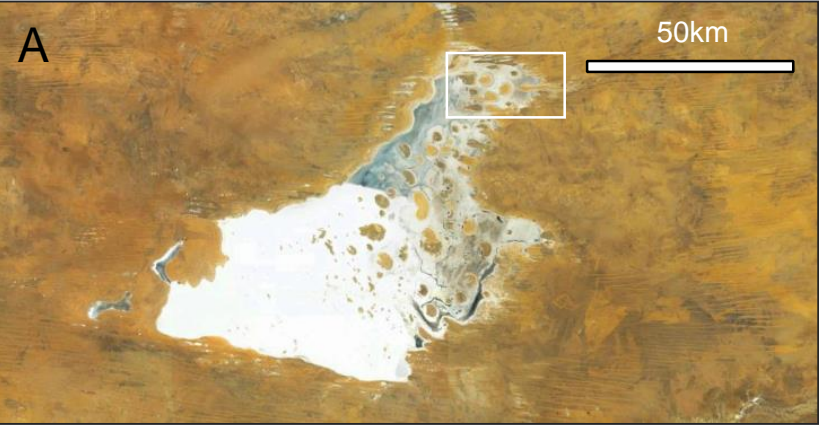
SUA/15/7/3	1.6	180-210	MG MAM	38	46.5 ± 5.8	0.180 ± 0.006	0.518	4.909	1.122	0.197	1.399 ± 0.14 ⁱ	130 ± 13
SUA/15/7/4	1.7	4-11	MGFG MAM	12	14.2 ± 5	51.2 ± 3.9	0.403	2.411	0.867	0.197	0.849 ± 0.05	60350 ± 5830

722 *Elemental concentrations all used with a 20% associated uncertainty. Sand mound ages were calculated using 10% moisture content and the

723 lake bed age used an average 25% moisture content. MG MAM = Multigrain Minimum Age Model; SG CAM = Single grain Central Age Model

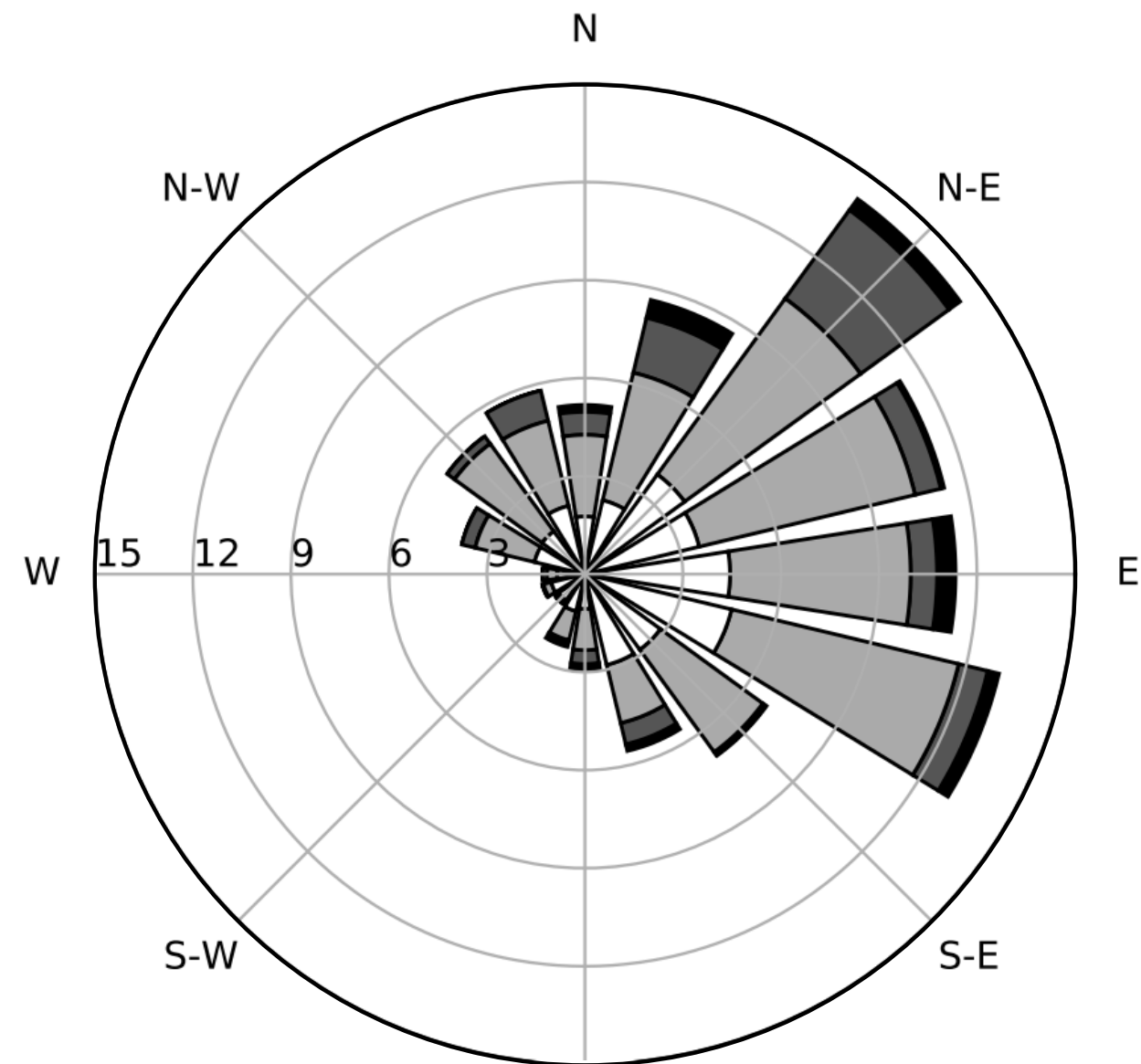
724

725 ⁱGamma dose calculated as an average of surrounding sandy sediment and underlying lake bed silts (SUA/15/7/4





Sua Pan



Model

